

## Synthesis and magnetic properties of the Shastry-Sutherland family $R_2\text{Be}_2\text{SiO}_7$ ( $R = \text{Nd}, \text{Sm}, \text{Gd-Yb}$ )

A. Brassington<sup>1</sup>,<sup>1</sup> Q. Huang,<sup>1</sup> A. A. Aczel<sup>2,\*</sup> and H. D. Zhou<sup>1,†</sup>

<sup>1</sup>*Department of Physics and Astronomy, University of Tennessee, Knoxville, Tennessee 37996, USA*

<sup>2</sup>*Neutron Scattering Division, Oak Ridge National Laboratory, Oak Ridge, Tennessee 37831, USA*



(Received 28 September 2023; accepted 28 November 2023; published 18 January 2024)

Compounds forming the quasi-two-dimensional Shastry-Sutherland lattice (SSL) have attracted significant experimental and theoretical attention in the field of frustrated magnetism. This is primarily due to their realization of an exactly soluble  $J_1$ - $J_2$  orthogonal dimer model capable of hosting magnetic order, dimer singlet, and plaquette singlet phases in zero applied field and their complex magnetic phase diagrams with fractional magnetization plateaus and possible superfluid and supersolid phases found between the plateau states. The discovery and characterization of SSL compounds based on rare-earth magnetic ions provide a direct route to study the stability and properties of these exotic magnetic phases in systems with a variety of different magnetic anisotropies. In this paper, we discuss the synthesis and magnetic characterization of polycrystalline samples of the  $R_2\text{Be}_2\text{SiO}_7$  family, where  $R = \text{Nd}, \text{Sm},$  and  $\text{Gd-Yb}$ . All family members crystallize in the space group  $P4_2/m$  (113) and show no signs of long-range magnetic order above 2 K, except for  $R = \text{Tb}$  which orders antiferromagnetically at 2.6 K.

DOI: [10.1103/PhysRevMaterials.8.014005](https://doi.org/10.1103/PhysRevMaterials.8.014005)

### I. INTRODUCTION

Materials with a combination of geometric frustration, low dimensionality, and spin- $\frac{1}{2}$  (or effective spin- $\frac{1}{2}$ ) magnetic ions have demonstrated a unique potential to escape conventional magnetic order and realize exotic magnetic ground states such as the quantum spin liquid [1–9]. Several two-dimensional lattices with a tendency towards frustration have already been identified and intensely investigated both experimentally and theoretically. Notable examples include the kagome, honeycomb, and triangular lattices [6,10,11]. In the same vein, the Shastry-Sutherland lattice (SSL) based on an exactly soluble model has proven to be of interest [12].

The SSL consists of a plane of orthogonal dimers with intradimer exchange  $J_1$  and interdimer exchange  $J_2$ . As pointed out by its namesakes Shastry and Sutherland in 1981, it is equivalent to a square lattice where every other square has an additional diagonal bond [12]. Several theoretical works have shown that the magnetic ground state of SSL systems depends critically on the ratio  $J_1/J_2$ . When  $J_1/J_2$  is sufficiently large a product of dimer singlet states (i.e., a valence bond solid) is favored while for small  $J_1/J_2$  typical Néel antiferromagnetic order is realized [13,14]. Additionally, exotic ground states have been predicted near the boundary between the two extremes such as quantum spin liquids and plaquette singlet phases [15–17].

Since the 1981 debut of the SSL as a toy model, its most famous experimental realization has been  $\text{SrCu}_2(\text{BO}_3)_2$ , where the spin- $\frac{1}{2}$   $\text{Cu}^{2+}$  ions form a SSL in the  $ab$  plane

and achieve a dimer spin-singlet ground state [18–21]. Remarkably,  $\text{SrCu}_2(\text{BO}_3)_2$  with an estimated  $J_1/J_2 = 0.68$  [22] is close to the critical value of  $J_1/J_2$  required to realize two quantum phase transitions and it can be driven across these boundaries via the application of pressure [23]. With increasing pressure, this system first transitions to a plaquette singlet state and then to an antiferromagnetic Néel state. The magnetic phase diagram of  $\text{SrCu}_2(\text{BO}_3)_2$  is also quite rich, as several magnetization plateaus have been identified that can be described in the context of triplon crystallization [18,24].

Beyond  $\text{SrCu}_2(\text{BO}_3)_2$ , most SSL compounds contain magnetic rare-earth ( $R$ ) ions. The  $RB_4$  family represents the only known binary SSL compounds. As  $\text{SrCu}_2(\text{BO}_3)_2$ , members of this family have complex magnetic phase diagrams and fractional magnetization plateaus [25–30]. For ternary compounds, a large metallic family with the general formula  $R_2T_2X$  and structure type  $U_3\text{Si}_2$  have been identified and synthesized.  $R_2T_2X$  compounds with  $T(X) = \text{Si}$  (Al, Sc, Mg, Li), Ge (Mg, In, Al, Sn, Cd), Ni (Sn, Mg), Cu (In, Mg, Cd), Pd (In, Pb, Cd, Mg), and Pt (Rh, Pb) have been reported and can be found in the international crystal structure database. Only a small subset of the listed  $R_2T_2X$  compounds have had their magnetic properties investigated, with bulk characterization evidence for antiferromagnetic and ferromagnetic ground states [31–38] available in select cases. The Yb-based systems have the most complex electronic and magnetic properties, with intermediate valence states identified in  $\text{Yb}_2\text{Si}_2\text{Al}$  [39] and  $\text{Yb}_2\text{Pd}_2\text{In}$  [32] and quasi-one-dimensional quantum magnetism arising from weakly coupled spin chains found in  $\text{Yb}_2\text{Pt}_2\text{Pb}$  [40–42]. Other ternary SSL compounds that have been synthesized remain relatively unexplored including  $R_5T_2\text{Cd}$  [43],  $R_2P_3N_7$  [44], and  $RB_2C_2$  [45].

\*aczelaa@ornl.gov

†hzhou10@utk.edu

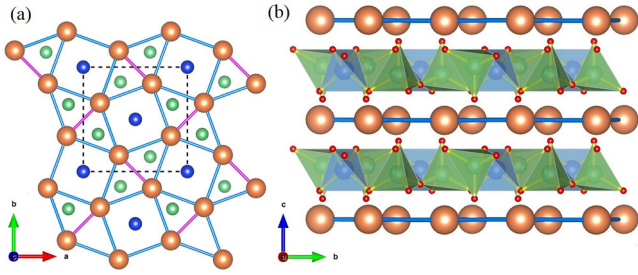


FIG. 1. (a) A schematic of the crystal structure for  $R_2Be_2SiO_7$  as seen perpendicular to the  $ab$  plane. The magnetic  $R^{3+}$  ions in orange form a Shastry-Sutherland lattice with an intradimer exchange  $J_1$  (pink bonds) and an interdimer exchange  $J_2$  (blue bonds). The non-magnetic  $Be^{2+}$  ions in green are arranged in a similar SSL structure. The  $Si^{4+}$  ions form a two-dimensional square lattice in the same plane as the  $Be^{2+}$  ions. (b) A schematic of the  $R_2Be_2SiO_7$  structure as viewed along the  $a$  axis. The  $SiO_4$  and  $BeO_4$  tetrahedra are shown in blue and green, respectively.

While most of the well-studied binary and ternary compounds are metallic, there are two known quaternary SSL families based on insulating oxides or sulfides with general formulas  $BaR_2MX_5$  ( $M = Pd, Zn; X = O, S$ ) [46–50] and the melilite type  $R_2Be_2GeO_7$  [51]. One key advantage of studying the insulating SSL systems is the theoretical  $J_1$ - $J_2$  model is more likely to be appropriate since

the interactions should have a superexchange rather than a longer-range Ruderman-Kittel-Kasuya-Yosida (RKKY) origin.  $BaNd_2ZnO_5$  and  $BaNd_2ZnS_5$  are Ising SSL systems that host noncollinear magnetic ground states below 3 K [46,49,50] consisting of ferromagnetic dimers with the moment direction lying in the  $ab$  plane perpendicular to the dimer bonds, with a partial suppression of this order observed in the sulfide sample at a moderate critical field  $H_c = 1.7$  T applied along the  $[1\bar{1}0]$  direction [52]. Bulk characterization measurements down to 2 K have been reported on  $R_2Be_2GeO_7$  [51] and several other members of the  $BaR_2MX_5$  family [47,48], with evidence for antiferromagnetic order identified in  $Tb_2Be_2GeO_7$  and several  $BaR_2PdO_5$  systems.

In this paper, we report the synthesis, crystal structures, and magnetic characterization of polycrystalline samples of  $R_2Be_2SiO_7$  ( $R = Nd, Sm, Gd$ -Yb), which represent a new SSL family that is isostructural to  $R_2Be_2GeO_7$ . We note that there has been one previous report on selected members of this family, which described the crystal growth and structural properties of  $Nd_2Be_2SiO_7$  and  $Ho_2Be_2SiO_7$  [53]. For the  $R_2Be_2SiO_7$  family, the  $R$  ions form a SSL in the  $ab$  plane as shown in Fig. 1(a). All family members crystallize in the tetragonal space group  $P4_21m$  (113). The SSL planes of rare-earth ions are separated by layers of nonmagnetic  $SiO_4$  and  $BeO_4$  tetrahedra as shown in Fig. 1(b). All family members have negative Curie-Weiss temperatures as expected for dominant antiferromagnetic intradimer interactions. Magnetic

TABLE I. Summary of room-temperature XRD Rietveld refinements for  $R_2Be_2SiO_7$  ( $R = Nd, Sm, Gd$ -Yb).

	Nd	Sm	Gd	Tb	Dy	Ho	Er	Tm	Yb
$R^{3+}$ IR (Å)	1.109	1.079	1.053	1.040	1.027	1.015	1.004	0.994	0.985
$a$ (Å)	7.46051(7)	7.40287(4)	7.35792(10)	7.33973(10)	7.30825(8)	7.28535(8)	7.25903(5)	7.24957(6)	7.22334(5)
$c$ (Å)	4.86246(4)	4.82202(3)	4.80066(6)	4.78005(6)	4.76866(6)	4.75659(5)	4.74094(4)	4.72797(4)	4.71925(3)
Dimer bond (Å)	3.3952(6)	3.3617(7)	3.3219(9)	3.3230(8)	3.3046(10)	3.2840(9)	3.2610(8)	3.2484(9)	3.2379(6)
Square bond (Å)	3.9601(6)	3.9312(7)	3.9003(8)	3.9001(8)	3.8844(10)	3.8749(9)	3.8635(8)	3.8606(7)	3.8462(6)
Interplane bond (Å)	4.862(3)	4.822(4)	4.801(6)	4.780(4)	4.769(6)	4.757(5)	4.741(5)	4.728(4)	4.719(3)
$R$	( $x, y, z$ )								
$x$	0.83910(6)	0.83945(7)	0.84038(9)	0.83993(8)	0.84013(10)	0.84063(9)	0.84117(8)	0.84158(9)	0.84152(6)
$y$	0.33910(6)	0.33945(7)	0.34038(9)	0.33993(8)	0.33013(10)	0.34063(9)	0.34117(8)	0.34158(9)	0.34152(6)
$z$	0.5011(5)	0.5002(6)	0.5025(9)	0.5042(6)	0.5028(9)	0.5048(7)	0.5037(7)	0.5047(6)	0.5039(5)
Si	(0,0,0)	(0,0,0)	(0,0,0)	(0,0,0)	(0,0,0)	(0,0,0)	(0,0,0)	(0,0,0)	(0,0,0)
Be	( $x, y, z$ )								
$x$	0.6416(15)	0.6481(18)	0.679(2)	0.645(2)	0.656(3)	0.643(2)	0.638(2)	0.621(2)	0.637(2)
$y$	0.1416(15)	0.1381(18)	0.179(2)	0.145(2)	0.156(3)	0.143(2)	0.138(2)	0.121(2)	0.137(2)
$z$	0.937(3)	0.943(3)	0.927(4)	0.940(3)	0.921(3)	0.947(4)	0.949(4)	0.959(5)	0.949(3)
$O_1$	( $x, y, z$ )								
$x$	0.9244(6)	0.9258(8)	0.9198(10)	0.9267(8)	0.9208(10)	0.9215(9)	0.9241(9)	0.9216(8)	0.9210(7)
$y$	0.8354(7)	0.8364(8)	0.8392(11)	0.8336(9)	0.8395(12)	0.8375(10)	0.8364(9)	0.8395(10)	0.8376(7)
$z$	0.1934(8)	0.1955(9)	0.1970(11)	0.2034(10)	0.2084(12)	0.1973(11)	0.2123(11)	0.2139(11)	0.2053(8)
$O_2$	( $x, y, z$ )								
$x$	0.6389(7)	0.6404(9)	0.6419(12)	0.6430(10)	0.6438(13)	0.6388(13)	0.6412(10)	0.6454(10)	0.6431(8)
$y$	0.1389(7)	0.1404(9)	0.1419(12)	0.1430(10)	0.1438(13)	0.1388(10)	0.1412(10)	0.1454(10)	0.1431(8)
$z$	0.2887(9)	0.2975(11)	0.2897(15)	0.3011(13)	0.2917(15)	0.2923(14)	0.2941(13)	0.2862(13)	0.2910(10)
$O_3$	( $0, \frac{1}{2}, z$ )								
$z$	0.169(2)	0.159(2)	0.186(3)	0.180(3)	0.170(3)	0.174(3)	0.156(3)	0.180(3)	0.163(2)
$R_p$	1.23	1.28	1.13	1.38	1.42	1.69	1.77	1.43	1.75
$R_{wp}$	1.70	1.81	1.51	1.97	2.15	2.76	2.85	2.19	2.72
$\chi^2$	1.69	2.19	1.46	2.57	3.02	3.83	4.19	2.42	3.79

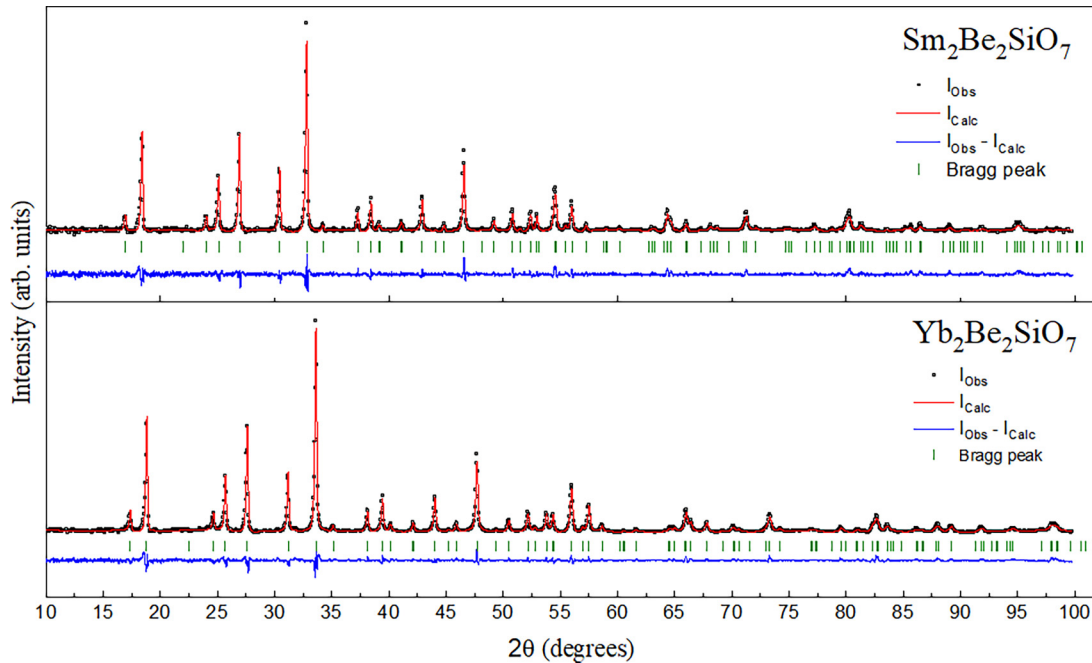


FIG. 2. Room-temperature XRD pattern of  $\text{Sm}_2\text{Be}_2\text{SiO}_7$  ( $\chi^2 = 2.96$ ) and  $\text{Yb}_2\text{Be}_2\text{SiO}_7$  ( $\chi^2 = 4.35$ ). Black circles represent experimental data, red curves show the calculated patterns, blue curves depict the difference plots, and green ticks indicate Bragg peaks.

susceptibility measurements reveal no signs of long-range order above 2 K, with the  $R = \text{Tb}$  system representing the lone exception with an antiferromagnetic transition identified at 2.6 K. Most family members, aside from the Gd compound, have high-field magnetization values that are significantly reduced from the free-ion limit, which emphasizes the importance of crystal-field effects. Due to its insulating nature and tunable magnetic anisotropy, the  $R_2\text{Be}_2\text{SiO}_7$  family represents an excellent opportunity to identify and characterize magnetic phenomena associated with the  $J_1$ - $J_2$  SSL model.

## II. EXPERIMENTAL DETAILS

Stoichiometric amounts of the appropriate rare-earth oxide (Strem Chemicals, 99.999%),  $\text{SiO}_2$  (Alfa Aesar, 99.8%), and  $\text{BeO}$  (Alfa Aesar, 99%) were ground and packed into a long cylindrical rod using a hydraulic press at a pressure of 40 psi. The cylindrical rods were then prereacted in air at  $1000^\circ\text{C}$  for 20 h in a conventional box oven. Next, they were reground and reacted twice in air at  $1300^\circ\text{C}$  for 20 h each time. For elements heavier than Dy, the reaction temperature was increased to  $1400^\circ\text{C}$ . Prior to use, all rare-earth oxides were preheated in air at  $1000^\circ\text{C}$  for at least 10 h.

The phase purity of the resulting polycrystalline powders was checked via room-temperature powder x-ray diffraction (XRD) using a HUBER imaging plate Guinier camera 670 with Cu radiation ( $\lambda = 1.54059 \text{ \AA}$ ). See Supplemental Material for .cif files [54]. No significant impurity phases were detected after the final reaction step although unknown impurity phases were observed during the intermediate grinding steps. The XRD refinements were performed with FULLPROF [55] using the structure of  $\text{Y}_2\text{Be}_2\text{SiO}_7$  as a starting reference [56]. The magnetic susceptibility and magnetization were measured in a Materials Property Measurement System

(MPMS) from Quantum Design with the vibrating superconducting quantum interference device (SQUID) magnetometer (VSM) option equipped. The crystal structures were plotted and the bond distances were computed using VESTA [57].

## III. RESULTS AND DISCUSSION

### A. Structural properties

All members of the  $R_2\text{Be}_2\text{SiO}_7$  family are isostructural and crystallize into the tetragonal space group  $P4_21m$  (113) with the melilite structure. There are six different crystallographic sites in the unit cell. The  $R$  and Be ions occupy two different  $4e$  Wyckoff sites that each generate a SSL. The Si ions occupy a  $2a$  Wyckoff site and they are found in the same plane as the Be ions, while the O ions occupy three different Wyckoff sites ( $2c$ ,  $4e$ , and  $8f$ ). The oxygen coordination of the  $R$ , Si, and Be ions is 8, 4, and 4, respectively. The distorted  $\text{RO}_8$  polyhedron generates a low-point symmetry of  $C_s$  (or  $m$ ), which needs to be taken into account when considering crystal-field splitting of the  $R$  ground-state multiplet. In  $\text{Dy}_2\text{Be}_2\text{SiO}_7$  the average Dy-O distance is  $2.414 \text{ \AA}$  compared to  $2.442 \text{ \AA}$  in  $\text{Dy}_2\text{Be}_2\text{GeO}_7$ , which indicates that the crystal-field effects on the Dy sites due to the surrounding oxygen ligands are expected to be similar in the two compounds. This finding is true regardless of the specific  $R$  ion being considered.

In this structure, the  $R$  and  $\text{BeO}_4/\text{SiO}_4$  planes are alternately stacked along the  $c$  axis as shown in Fig. 1(b). Each  $\text{BeO}_4/\text{SiO}_4$  plane is made up of a series of edge-sharing tetrahedra. While this atomic arrangement is reminiscent of the ternary compounds with the  $\text{U}_3\text{Si}_2$  structure such as  $\text{Yb}_2\text{Pt}_2\text{Pb}$ , the addition of the O ions between the  $R$  and cation layers ensures that the  $R_2\text{Be}_2\text{SiO}_7$  family is insulating. Taking  $\text{Gd}_2\text{Be}_2\text{SiO}_7$  as a representative example, the intradimer distance is  $3.3219 \text{ \AA}$ , the interdimer (square bond) distance is

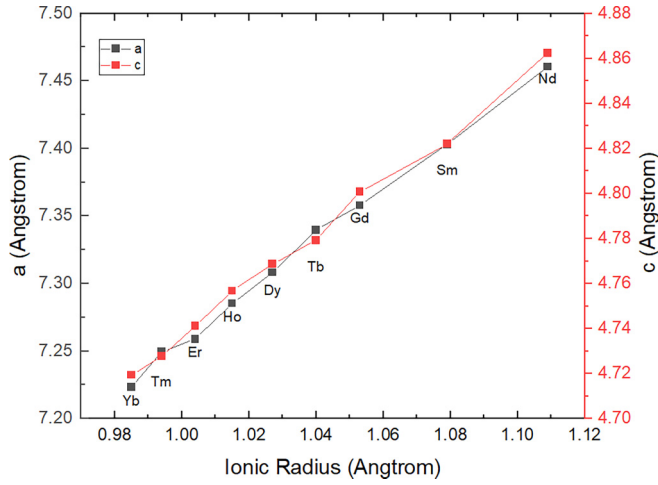


FIG. 3. The lattice parameters  $a$  (left axis) and  $c$  (right axis) vs rare-earth ionic radius (IR) from Shannon [58]. Both lattice constants increase approximately linearly with increasing ionic radius.

3.9003 Å, and the interplane distance is 4.801 Å. Since the interplane distance is much larger than the nearest-neighbor and next-nearest-neighbor in-plane distances in  $\text{Gd}_2\text{Be}_2\text{SiO}_7$

and the other members of this family, these materials can likely be modeled as quasi-two-dimensional magnets.

Detailed crystal structure refinement results and select distances are provided in Table I. Representative XRD patterns for  $R_2\text{Be}_2\text{SiO}_7$  ( $R = \text{Sm}, \text{Yb}$ ) with the refinement results superimposed on the data are shown in Fig. 2 and they agree well with the calculated pattern from the previous single-crystal study [53]. The XRD refinement results indicate no significant signs of  $\text{Be}^{2+}/\text{Si}^{4+}$  site mixing, which is in good agreement with previous work on  $R_2\text{Be}_2\text{GeO}_7$  [51]. Figure 3 shows the lattice parameters  $a$  (left axis) and  $c$  (right axis) versus ionic radius (IR) for all compounds synthesized in the  $R_2\text{Be}_2\text{SiO}_7$  series. The lattice constants increase approximately linearly with increasing  $R$  ionic radius.  $\text{Yb}_2\text{Be}_2\text{SiO}_7$  has the smallest unit cell with  $a = 7.223$  Å and  $c = 4.719$  Å while  $\text{Nd}_2\text{Be}_2\text{SiO}_7$  has the largest unit cell with  $a = 7.461$  Å and  $c = 4.862$  Å.

## B. Magnetic properties

The temperature dependences of the magnetic susceptibilities  $\chi$  (plotted as magnetization/field  $M/H$ ) vs  $T$  for the family  $R_2\text{Be}_2\text{SiO}_7$  were measured under a 0.1 T field using zero-field cooling. Similarly to the  $R_2\text{Be}_2\text{SiO}_7$  fam-

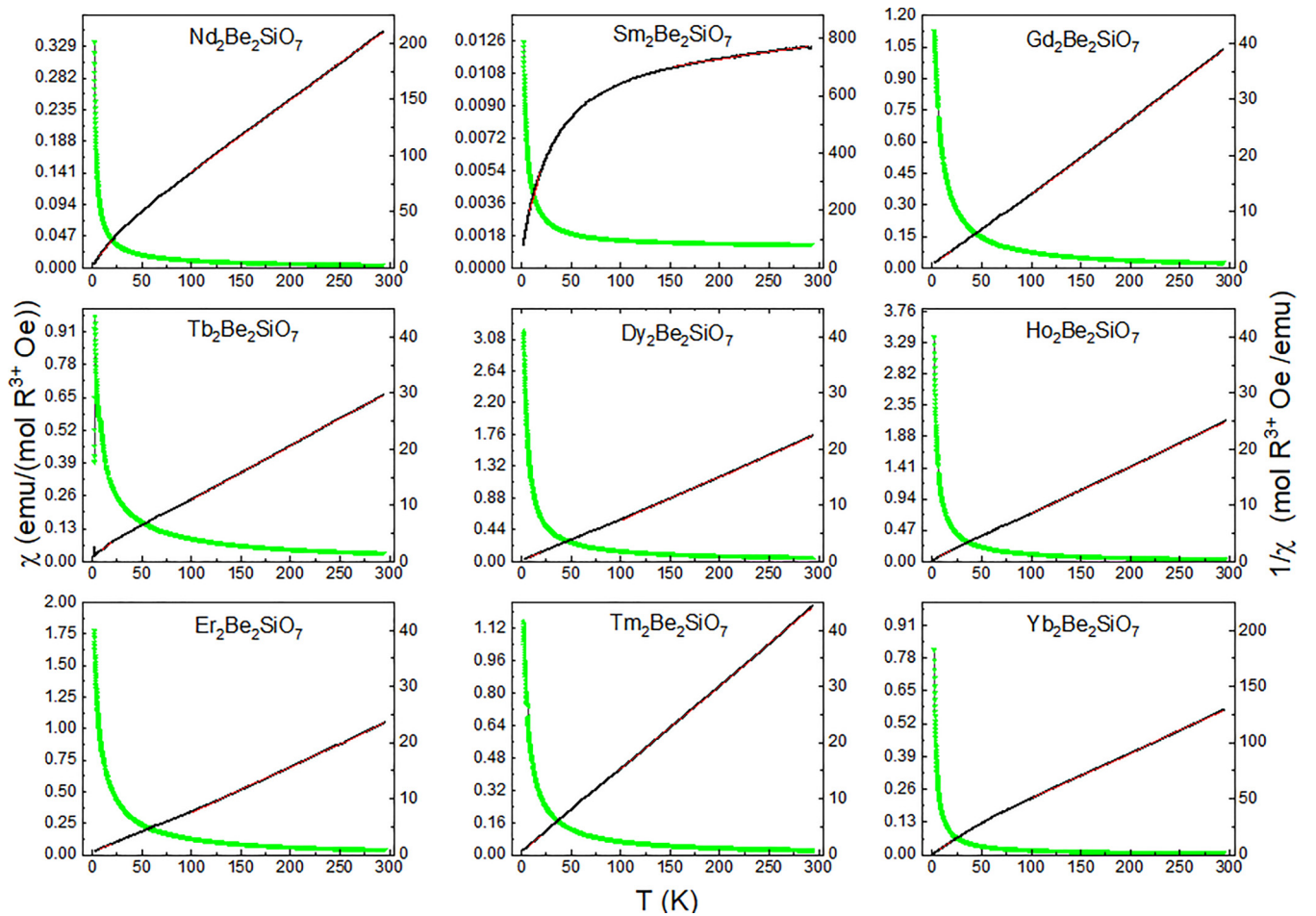


FIG. 4. Susceptibility ( $\chi$ , left axis) and inverse susceptibility ( $1/\chi$ , right axis) vs temperature under a dc field of 0.1 T for  $R_2\text{Be}_2\text{SiO}_7$  ( $R = \text{Nd}, \text{Sm}, \text{Gd}, \text{Yb}$ ). The red lines correspond to the regions of the low- and high-temperature Curie-Weiss fits. The  $R = \text{Tb}$  sample shows a clear peak at about 2.6 K, which likely arises from a transition to long-range antiferromagnetic order. All other compounds show no signs of long-range order above 2 K.

TABLE II. Summary of magnetism parameters for  $R_2\text{Be}_2\text{SiO}_7$  ( $R = \text{Nd, Sm, Gd-Yb}$ ).

$R$	High- $T$ fit (K)	$\theta_{\text{cw}}$ (K)	$\mu_{\text{eff}}(\mu_B)$	Low- $T$ fit (K)	$\theta_{\text{cw}}$ (K)	$\mu_{\text{eff}}(\mu_B)$	$\mu_{\text{cal}}(\mu_B)$	$g_{JJ}(\mu_B)$	$M_{12\text{T}}(\mu_B)$
Nd	100–290	−31.79(6)	3.52(7)	8–20	−2.32(6)	2.67(19)	3.62	3.273	1.22
Sm	150–290	−1193(2)	3.92(7)	8–20	−8.2(1.1)	0.81(8)	0.85	0.714	0.16
Gd	100–290	2.61(4)	7.748(2)	8–20	−5.11(4)	8.044(7)	7.94	7	6.74
Tb	100–290	−14.09(4)	9.114(1)	10–20	−5.52(17)	7.665(15)	9.72	9	4.28
Dy	100–290	4.94(6)	10.174(1)	8–20	−1.92(3)	10.336(3)	10.65	10	5.20
Ho	100–290	−0.57(7)	9.756(1)	8–20	−2.38(4)	9.428(4)	10.61	10	5.78
Er	100–290	7.73(10)	9.905(2)	8–20	−7.64(7)	10.560(4)	9.58	9	7.04
Tm	100–290	−1.85(6)	7.321(3)	8–20	−3.49(3)	7.291(8)	7.56	7	3.46
Yb	100–290	−24.49(7)	4.45(1)	8–20	−0.86(3)	3.69(6)	4.54	4	1.91

ily [51], only  $\text{Tb}_2\text{Be}_2\text{SiO}_7$  shows signatures of a transition to long-range antiferromagnetic order at  $T_N = 2.6$  K. The Curie-Weiss law ( $1/\chi = T/C - \theta_{\text{cw}}/C$  [59]) was used to fit the inverse susceptibility ( $1/\chi$ ) as shown in Fig. 4, where  $C$  and  $\theta_{\text{cw}}/C$  were extracted from the slope and the y intercept respectively. From these values  $\theta_{\text{cw}}$ ,  $\mu_{\text{eff}} = \sqrt{8C}\mu_B$ , and  $\mu_{\text{cal}} = g_J\sqrt{J(J+1)}\mu_B$  were obtained and they can be found in Table II.

The high-temperature fits were performed between 100 and 290 K and the low-temperature fits used the 8–20 K data for most systems, unless specified otherwise in Table II. The high-temperature Curie-Weiss fitting was performed from 150 to 290 K for the Sm sample due to the significant curvature in the  $T$  dependence of the  $1/\chi$  plot that arises from the small gap between the crystal-field ground-state multiplet  $J = \frac{5}{2}$  and first excited multiplet  $J = \frac{7}{2}$  [60]. A different low-temperature fitting range was chosen for the Tb sample due to the low-temperature magnetic transition. At high temperatures, the fitted effective moments  $\mu_{\text{eff}}$  are close to the free-ion values  $\mu_{\text{cal}}$ . The slope of  $1/\chi$  changes as the temperature decreases, which is particularly prominent in the Nd, Sm, and Yb samples. The low-temperature Curie-Weiss fitting reveals negative  $\theta_{\text{cw}}$  values for all compounds, likely arising from dominant antiferromagnetic intradimer interactions. The effective magnetic moments also decrease significantly in some cases, particularly for the Nd, Sm, Tb, and Yb samples, as the crystal-field ground state and low-lying excitations become more populated with decreasing temperature.

The dipolar interactions  $D = \mu_0\mu_{\text{eff}}^2/4\pi r^3$  for various pairs of  $R^{3+}$  ions in the crystal structure ( $D_{ab1}$ : intradimer;  $D_{ab2}$ : interdimer; and  $D_c$ : interplane) are shown in Table III. Here,  $r$  is the relevant bond length between  $R^{3+}$  ions and an estimate of  $\mu_{\text{eff}}$  is obtained from the low- $T$  Curie-Weiss fit. The average strength of the superexchange interactions between  $R^{3+}$  ions in a given  $ab$  plane are also shown in Table III. These values were estimated using the mean field approximation  $J_{ab} = 3k_B\theta_{\text{cw}}/zJ_{\text{eff}}(J_{\text{eff}} + 1)$  where  $\theta_{\text{cw}}$  is obtained from the low- $T$   $1/\chi$  fits,  $z = 5$  is the number of neighboring  $R^{3+}$  ions (both intradimer and interdimer bonds), and  $J_{\text{eff}} = \frac{1}{2}$  or  $J$  (the free-ion value determined by Hund's rules). The dipolar interaction strength between the  $R^{3+}$  ions in neighboring layers is typically weaker than the in-plane interaction strengths. For all compounds  $D_c/D_{ab1} \approx 0.3$  while  $D_{ab2}/D_{ab1} \approx 0.6$ . The average in-plane superexchange interaction is significantly weaker than the dipolar interaction in the  $J_{\text{eff}} = J$  case but is expected to be a significant if not dominant interaction in the  $J_{\text{eff}} = 1/2$  case.

The isothermal magnetization curves collected at 2 K for several  $R_2\text{Be}_2\text{SiO}_7$  systems are shown in Figs. 5(a) and 5(b). For the Tb sample, the abrupt change in the slope of the magnetization around 0.5 T is likely indicative of a metamagnetic transition. A similar feature was observed in the magnetization data for  $\text{Tb}_2\text{Be}_2\text{GeO}_7$  [51]. Members are grouped either as Kramers ( $R = \text{Nd, Sm, Gd, Dy, Er, Yb}$ ) or non-Kramers ions ( $R = \text{Tb, Ho, Tm}$ ). Kramers ions are guaranteed by time-reversal symmetry constraints to have a crystal-field ground state with a degeneracy of two or higher precluding the possibility of a single-ion singlet state and enabling effective

TABLE III. Dipolar interaction strengths ( $D_{ab1}$ : in-plane nearest neighbors;  $D_{ab2}$ : in-plane next-nearest neighbors; and  $D_c$ : out-of-plane nearest neighbors) and average in-plane exchange constants  $J_{ab}$  for the  $R$  ions of the series  $R_2\text{Be}_2\text{SiO}_7$  ( $R = \text{Nd, Sm, Gd-Yb}$ ).

$R$	$D_{ab2}$ (K)	$D_{ab1}$ (K)	$D_c$ (K)	$J_{ab}$ (K) using $J$	$J_{ab}$ (K) using $J_{\text{eff}} = 1/2$
Nd	0.132	0.207	0.071	0.0582	1.92
Sm	$7.39 \times 10^{-3}$	0.012	$4 \times 10^{-3}$	0.560	6.54
Gd	0.668	1.06	0.360	0.195	4.09
Tb	0.696	1.13	0.378	0.0746	4.18
Dy	1.132	1.836	0.605	0.0181	1.54
Ho	0.929	1.506	0.497	0.0198	1.90
Er	1.165	1.909	0.629	0.0719	6.11
Tm	0.572	0.959	0.311	0.0499	2.79
Yb	0.145	0.238	0.078	0.0328	0.688

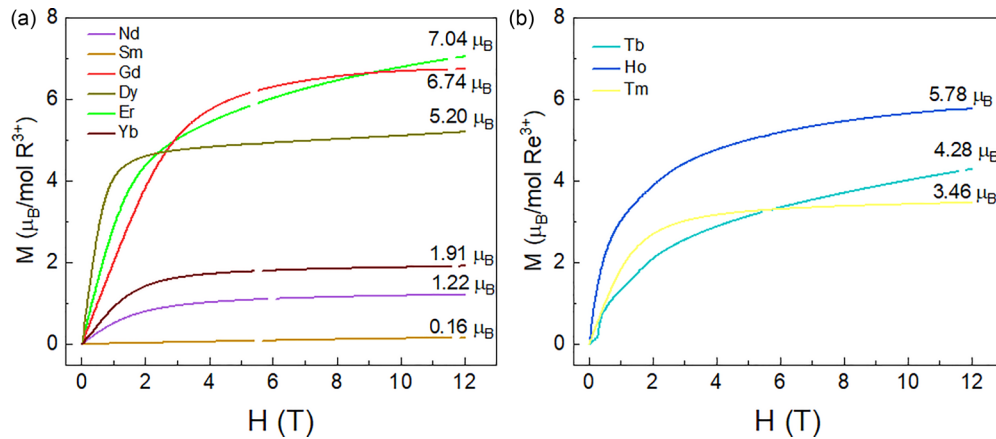


FIG. 5. Field dependence of magnetization at 2 K under zero-field cooling for  $R_2\text{Be}_2\text{SiO}_7$  ( $R = \text{Nd, Sm, Gd-Yb}$ ). The data for the Kramers ions and non-Kramers ions are plotted in (a) and (b), respectively.

spin- $\frac{1}{2}$  physics to be realized in select cases. Non-Kramers ions lack this constraint and may host singlet ground states, particularly in the present case where the rare-earth sites have low-point symmetry. The half-filled  $4f$  subshell of the Gd system ensures that it is the lone system which  $M_{12\text{T}}/g_{JJ}$  close to 1 and Heisenberg anisotropy. The magnetization of most other compounds saturates well before 12 T, with reduced saturation moments compared to the free-ion values  $g_{JJ}$  due to crystal-field effects. There are also small linear increases in the high-field regime that are apparent in select cases due to weak van Vleck paramagnetism. On the other hand, the Er, Tb, and Ho compounds display significant nonlinear field dependence in the high-field magnetization which likely arises from low-lying crystal-field level contributions. For the Tm and Yb samples, the high-field magnetization saturates at a value of  $M_{12\text{T}}/(g_{JJ})$  close to  $\frac{1}{2}$ . For rare-earth pyrochlore systems such as  $\text{Dy}_2\text{Ti}_2\text{O}_7$  and  $\text{Ho}_2\text{Ti}_2\text{O}_7$  [61] this behavior can be explained by a  $J_{\text{eff}} = 1/2$  Ising model, but more work needs to be done to determine if a similar model is applicable to the current systems. In particular, neutron spectroscopy data will be beneficial for accurately determining the crystal-field level schemes and ground-state magnetic anisotropies of their rare-earth moments.

#### IV. CONCLUSIONS

A new family of Shastry-Sutherland lattice rare-earth compounds  $R_2\text{Be}_2\text{SiO}_7$  has been synthesized and characterized.

All members of the family are isostructural and crystallize into space group  $P\bar{4}2_1m$  (113). The rare-earth ions form the Shastry-Sutherland lattice in the  $ab$  plane and are AAA stacked along the  $c$  axis. X-ray diffraction refinement results are consistent with previously reported single-crystal data on  $\text{Nd}_2\text{Be}_2\text{SiO}_7$  and  $\text{Ho}_2\text{Be}_2\text{SiO}_7$ . The susceptibility and magnetization measurements indicate no signs of long-range magnetic order above 2 K, except for the Tb sample, which shows evidence of an antiferromagnetic transition at  $T_N = 2.6$  K. The magnetization data also suggest that the Gd system has Heisenberg anisotropy and several other systems have low-lying crystal-field levels. Neutron spectroscopy measurements will be invaluable for establishing the single-ion ground states of these systems, while low-temperature bulk characterization and neutron diffraction work will facilitate the exploration of magnetic phenomena associated with the  $J_1$ - $J_2$  Shastry-Sutherland lattice in both zero and applied magnetic fields.

#### ACKNOWLEDGMENTS

We thank Q. Ma and G. Sala for useful discussions. Research at the University of Tennessee is supported by the National Science Foundation, Division of Materials Research under Award No. NSF-DMR-2003117. The work of one of the authors (A.A.A.) was funded by the U.S. Department of Energy, Office of Science, Basic Energy Sciences.

- [1] L. Balents, Spin liquids in frustrated magnets, *Nature (London)* **464**, 199 (2010).
- [2] M. R. Norman, Colloquium: Herbertsmithite and the search for the quantum spin liquid, *Rev. Mod. Phys.* **88**, 041002 (2016).
- [3] L. Savary and L. Balents, Quantum spin liquids: a review, *Rep. Prog. Phys.* **80**, 016502 (2017).
- [4] Y. Zhou, K. Kanoda, and T.-K. Ng, Quantum spin liquid states, *Rev. Mod. Phys.* **89**, 025003 (2017).
- [5] J. Knolle and R. Moessner, A field guide to spin liquids, *Annu. Rev. Condens. Matter Phys.* **10**, 451 (2019).
- [6] H. Takagi, T. Takayama, G. Jackeli, G. Khaliullin, and S. E. Nagler, Concept and realization of Kitaev quantum spin liquids, *Nat. Rev. Phys.* **1**, 264 (2019).
- [7] J. Wen, S.-L. Yu, S. Li, W. Yu, and J.-X. Li, Experimental identification of quantum spin liquids, *npj Quantum Mater.* **4**, 12 (2019).
- [8] C. Broholm, R. J. Cava, S. A. Kivelson, D. G. Nocera, M. R. Norman, and T. Senthil, Quantum spin liquids, *Science* **367**, eaay0668 (2020).
- [9] J. R. Chamorro, T. M. McQueen, and T. T. Tran, Chemistry of quantum spin liquids, *Chem. Rev.* **121**, 2898 (2021).

- [10] J. E. Greedan, Geometrically frustrated magnetic materials, *J. Mater. Chem.* **11**, 37 (2001).
- [11] O. A. Starykh, Unusual ordered phases of highly frustrated magnets: a review, *Rep. Prog. Phys.* **78**, 052502 (2015).
- [12] B. S. Shastry and B. Sutherland, Exact ground state of a quantum mechanical antiferromagnet, *Physica B+C* **108**, 1069 (1981).
- [13] S. Miyahara and K. Ueda, Theory of the orthogonal dimer Heisenberg spin model for  $\text{SrCu}_2(\text{BO}_3)_2$ , *J. Phys.: Condens. Matter.* **15**, R327 (2003).
- [14] A. Vasiliev, O. Volkova, E. Zvereva, and M. Markina, Milestones of low-D quantum magnetism, *npj Quantum Mater.* **3**, 18 (2018).
- [15] S. Moukouri, Plaquette ground state of the Shastry-Sutherland model: Density-matrix renormalization-group calculations, *Phys. Rev. B* **78**, 132405 (2008).
- [16] J. Yang, A. W. Sandvik, and L. Wang, Quantum criticality and spin liquid phase in the Shastry-Sutherland model, *Phys. Rev. B* **105**, L060409 (2022).
- [17] J. Wang, H. Li, N. Xi, Y. Gao, Q.-B. Yan, W. Li, and G. Su, Plaquette singlet transition, magnetic barocaloric effect, and spin supersolidity in the Shastry-Sutherland model, *Phys. Rev. Lett.* **131**, 116702 (2023).
- [18] H. Kageyama, K. Yoshimura, R. Stern, N. V. Mushnikov, K. Onizuka, M. Kato, K. Kosuge, C. P. Slichter, T. Goto, and Y. Ueda, Exact dimer ground state and quantized magnetization plateaus in the two-dimensional spin system  $\text{SrCu}_2(\text{BO}_3)_2$ , *Phys. Rev. Lett.* **82**, 3168 (1999).
- [19] H. Kageyama, K. Onizuka, T. Yamauchi, Y. Ueda, S. Hane, H. Mitamura, T. Goto, K. Yoshimura, and K. Kosuge, Anomalous magnetizations in single crystalline  $\text{SrCu}_2(\text{BO}_3)_2$ , *J. Phys. Soc. Jpn.* **68**, 1821 (1999).
- [20] H. Kageyama, M. Nishi, N. Aso, K. Onizuka, T. Yoshida, K. Nukui, K. Kodama, K. Kakurai, and Y. Ueda, Direct evidence for the localized single-triplet excitations and the dispersive multitriplet excitations in  $\text{SrCu}_2(\text{BO}_3)_2$ , *Phys. Rev. Lett.* **84**, 5876 (2000).
- [21] B. D. Gaulin, S. H. Lee, S. Haravifard, J. P. Castellán, A. J. Berlinsky, H. A. Dabkowska, Y. Qiu, and J. R. D. Copley, High-resolution study of spin excitations in the singlet ground state of  $\text{SrCu}_2(\text{BO}_3)_2$ , *Phys. Rev. Lett.* **93**, 267202 (2004).
- [22] S. Miyahara and K. Ueda, Exact dimer ground state of the two dimensional heisenberg spin system  $R = \text{SrCu}_2(\text{BO}_3)_2$ , *Phys. Rev. Lett.* **82**, 3701 (1999).
- [23] M. E. Zayed, C. Rüegg, J. Larrea J., A. M. Läuchli, C. Panagopoulos, S. S. Saxena, M. Ellerby, D. F. McMorrow, T. Strässle, S. Klotz, G. Hamel, R. A. Sadykov, V. Pomjakushin, M. Boehm, M. Jiménez-Ruiz, A. Schneidewind, E. Pomjakushina, M. Stingaciu, K. Conder, and H. M. Rønnow, 4-spin plaquette singlet state in the Shastry-Sutherland compound  $\text{SrCu}_2(\text{BO}_3)_2$ , *Nat. Phys.* **13**, 962 (2017).
- [24] S. Sebastian, N. Harrison, P. Sengupta, C. Batista, S. Francoual, E. Palm, T. Murphy, N. Marcano, H. Dabkowska, and B. D. Gaulin, Fractalization drives crystalline states in a frustrated spin system, *Proc. Natl. Acad. Sci. USA* **105**, 20157 (2008).
- [25] S. Michimura, A. Shigekawa, F. Iga, M. Sera, T. Takabatake, K. Ohoyama, and Y. Okabe, Magnetic frustrations in the Shastry-Sutherland system  $\text{ErB}_4$ , *Phys. B: Condens. Matter* **378-380**, 596 (2006).
- [26] S. Yoshii, T. Yamamoto, M. Hagiwara, A. Shigekawa, S. Michimura, F. Iga, T. Takabatake, and K. Kindo, High-field magnetization of  $\text{TmB}_4$ , *J. Phys.: Conf. Ser.* **51**, 59 (2006).
- [27] S. Yoshii, T. Yamamoto, M. Hagiwara, S. Michimura, A. Shigekawa, F. Iga, T. Takabatake, and K. Kindo, Multistep magnetization plateaus in the Shastry-Sutherland system  $\text{TbB}_4$ , *Phys. Rev. Lett.* **101**, 087202 (2008).
- [28] J. Y. Kim, B. K. Cho, and S. H. Han, Anisotropic magnetic phase diagrams of  $\text{HoB}_4$  single crystal, *J. Appl. Phys.* **105**, 07E116 (2009).
- [29] L. Ye, T. Suzuki, and J. G. Checkelsky, Electronic transport on the Shastry-Sutherland lattice in Ising-type rare-earth tetraborides, *Phys. Rev. B* **95**, 174405 (2017).
- [30] D. Brunt, G. Balakrishnan, D. A. Mayoh, M. R. Lees, D. Gorbunov, N. Qureshi, and O. A. Petrenko, Magnetisation process in the rare earth tetraborides,  $\text{NdB}_4$  and  $\text{HoB}_4$ , *Sci. Rep.* **8**, 232 (2018).
- [31] F. Hulliger, On new  $\text{Mo}_2\text{FeB}_2$ -type representatives  $\text{Ln}_2\text{Rh}_2\text{In}$ , *J. Alloys Compd.* **221**, L11 (1995).
- [32] M. Giovannini, H. Michor, E. Bauer, G. Hilscher, P. Rogl, and R. Ferro, Structural chemistry, magnetism and thermodynamic properties of  $R_2\text{Pd}_2\text{In}$ , *J. Alloys Compd.* **280**, 26 (1998).
- [33] R. Kraft, T. Fickenscher, G. Kotzyba, R.-D. Hoffmann, and R. Pöttgen, Intermetallic rare earth (RE) magnesium compounds  $\text{REPdMg}$  and  $\text{RE}_2\text{Pd}_2\text{Mg}$ , *Intermetallics* **11**, 111 (2003).
- [34] V. I. Zaremba, D. Kaczorowski, G. P. Nychyporuk, U. C. Rodewald, and R. Pöttgen, Structure and physical properties of  $\text{RE}_2\text{Ge}_2\text{In}$  ( $\text{RE} = \text{La}, \text{Ce}, \text{Pr}, \text{Nd}$ ), *Solid State Sci.* **6**, 1301 (2004).
- [35] S. Rayaprol, A. Doğan, and R. Pöttgen, Magnetic properties and specific heat studies of  $\text{RE}_2\text{Pd}_2\text{Cd}$  ( $\text{RE} = \text{La}, \text{Ce}, \text{Nd}$ ), *J. Phys.: Condens. Matter* **18**, 5473 (2006).
- [36] F. M. Schappacher, W. Hermes, and R. Pöttgen, Structure and magnetic properties of  $\text{RE}_2\text{Cu}_2\text{Cd}$ , *J. Solid State Chem.* **182**, 265 (2009).
- [37] K. V. Shah, P. Bonville, P. Manfrinetti, F. Wrubl, and S. K. Dhar, The  $\text{Yb}_2\text{Al}_{1-x}\text{Mg}_x\text{Si}_2$  series from a spin fluctuation ( $x = 0$ ) to a magnetically ordered ground state ( $x = 1$ ), *J. Phys.: Condens. Matter* **21**, 176001 (2009).
- [38] N.-T. Suen, P. H. Tobash, and S. Bobev, Synthesis, structural characterization and magnetic properties of  $\text{RE}_2\text{MgGe}_2$  ( $\text{RE} = \text{rare-earth metal}$ ), *J. Solid State Chem.* **184**, 2941 (2011).
- [39] W. J. Gannon, K. Chen, M. Sundermann, F. Strigari, Y. Utsumi, K.-D. Tsuei, J.-P. Rueff, P. Bencok, A. Tanaka, A. Severing, and M. C. Aronson, Intermediate valence in single crystalline  $\text{Yb}_2\text{Si}_2\text{Al}$ , *Phys. Rev. B* **98**, 075101 (2018).
- [40] W. Miller, L. S. Wu, M. S. Kim, T. Orvis, J. W. Simonson, M. Gamza, D. M. McNally, C. S. Nelson, G. Ehlers, A. Podlesnyak, J. S. Helton, Y. Zhao, Y. Qiu, J. R. D. Copley, J. W. Lynn, I. Zaliznyak, and M. C. Aronson, Magnetic structure of  $\text{Yb}_2\text{Pt}_2\text{Pb}$ : Ising moments on the Shastry-Sutherland lattice, *Phys. Rev. B* **93**, 104419 (2016).
- [41] L. Wu, W. Gannon, I. Zaliznyak, A. Tsvelik, M. Brockmann, J. Caux, M. S. Kim, Y. Qiu, J. Copley, G. Ehlers, A. Podlesnyak, and M. Aronson, Orbital-exchange and fractional quantum number excitations in an  $f$ -electron metal,  $\text{Yb}_2\text{Pt}_2\text{Pb}$ , *Science* **352**, 1206 (2016).
- [42] W. J. Gannon, I. A. Zaliznyak, L. S. Wu, A. E. Feiguin, A. M. Tsvelik, F. Demmel, Y. Qiu, J. R. D. Copley, M. S. Kim, and M. C. Aronson, Spinon confinement and a sharp longitudinal

- mode in  $\text{Yb}_2\text{Pt}_2\text{Pb}$  in magnetic fields, *Nat. Commun.* **10**, 1123 (2019).
- [43] F. Tappe, C. Schwickert, M. Eul, and R. Pöttgen, Intermetallic cadmium compounds  $M_5T_2\text{Cd}$  ( $M = \text{Ca}, \text{Yb}, \text{Eu}$ ;  $T = \text{Cu}, \text{Ag}, \text{Au}$ ) with  $\text{Mo}_5\text{B}_2\text{Si}$ -type structure, *Zeitschrift für Naturforschung B* **66**, 1219 (2011).
- [44] S. D. Kloß, N. Weidmann, R. Niklaus, and W. Schnick, High-pressure synthesis of melilite-type rare-earth nitridophosphates  $\text{RE}_2\text{P}_3\text{N}_7$  and a  $\text{Ba}_2\text{CuSi}_2\text{O}_7$ -type polymorph, *Inorg. Chem.* **55**, 9400 (2016).
- [45] K. Ohoyama, K. Kaneko, K. Indoh, H. Yamauchi, A. Tobo, H. Onodera, and Y. Yamaguchi, Systematic study on crystal structures in tetragonal  $\text{RB}_2\text{C}_2$  ( $R = \text{rare earth}$ ) compounds, *J. Phys. Soc. Jpn.* **70**, 3291 (2001).
- [46] M. Wakeshima, N. Taira, Y. Hinatsu, A. Tobo, K. Ohoyama, and Y. Yamaguchi, Specific heat and neutron diffraction study on quaternary sulfides  $\text{BaNd}_2\text{CoS}_5$  and  $\text{BaNd}_2\text{ZnS}_5$ , *J. Solid State Chem.* **174**, 159 (2003).
- [47] T. Ozawa, T. Taniguchi, Y. Kawaji, S. Mizusaki, Y. Nagata, Y. Noro, H. Samata, H. Mitamura, and S. Takayanagi, Magnetization and specific heat measurement of the Shastry–Sutherland lattice compounds:  $\text{Ln}_2\text{BaPdO}_5$  ( $\text{Ln} = \text{La}, \text{Pr}, \text{Nd}, \text{Sm}, \text{Eu}, \text{Gd}, \text{Dy}, \text{Ho}$ ), *J. Alloys Compd.* **448**, 96 (2008).
- [48] Y. Ishii, J. Chen, H. K. Yoshida, M. Oda, A. D. Christianson, and K. Yamaura, High-pressure synthesis, crystal structure, and magnetic properties of the Shastry-Sutherland-lattice oxides  $\text{BaLn}_2\text{ZnO}_5$  ( $\text{Ln} = \text{Pr}, \text{Sm}, \text{Eu}$ ), *J. Solid State Chem.* **289**, 121489 (2020).
- [49] Y. Ishii, G. Sala, M. B. Stone, V. O. Garlea, S. Calder, J. Chen, H. K. Yoshida, S. Fukuoka, J. Yan, C. dela Cruz, M.-H. Du, D. S. Parker, H. Zhang, C. D. Batista, K. Yamaura, and A. D. Christianson, Magnetic properties of the Shastry-Sutherland lattice material  $\text{BaNd}_2\text{ZnO}_5$ , *Phys. Rev. Mater.* **5**, 064418 (2021).
- [50] B. R. Billingsley, M. Marshall, Z. Shu, H. Cao, and T. Kong, Single crystal synthesis and magnetic properties of a Shastry-Sutherland lattice compound  $\text{BaNd}_2\text{ZnS}_5$ , *Phys. Rev. Mater.* **6**, 104403 (2022).
- [51] M. Ashtar, Y. Bai, L. Xu, Z. Wan, Z. Wei, Y. Liu, M. A. Marwat, and Z. Tian, Structure and magnetic properties of melilite-type compounds  $\text{RE}_2\text{Be}_2\text{GeO}_7$  ( $\text{RE} = \text{Pr}, \text{Nd}, \text{Gd-Yb}$ ) with rare-earth ions on the Shastry–Sutherland lattice, *Inorg. Chem.* **60**, 3626 (2021).
- [52] M. Marshall, B. R. Billingsley, X. Bai, Q. Ma, T. Kong, and H. Cao, Field-induced partial disorder in a Shastry-Sutherland lattice, *Nat. Commun.* **14**, 3641 (2023).
- [53] C. Müller and H. Müller-Buschbaum, Zwei oxometallate mit melilith-struktur:  $\text{Nd}_2\text{SiBe}_2\text{O}_7$  und  $\text{Ho}_2\text{SiBe}_2\text{O}_7$ , *J. Alloys Compd.* **199**, 151 (1993).
- [54] See Supplemental Material at <http://link.aps.org/supplemental/10.1103/PhysRevMaterials.8.014005> for .cif files produced from room-temperature XRD refinements.
- [55] J. Rodríguez-Carvajal, Recent advances in magnetic structure determination by neutron powder diffraction, *Phys. B: Condens. Matter* **192**, 55 (1993).
- [56] G. M. Kuz'micheva, V. B. Rybakov, S. A. Kutovoi, V. L. Panyutin, A. Yu. Oleinik, and O. G. Plashkare, Preparation, structure, and properties of new laser crystals  $\text{Y}_2\text{SiBe}_2\text{O}_7$  and  $\text{Y}_2\text{Al}(\text{BeB})\text{O}_7$ , *Inorg. Mater.* **38**, 60 (2002).
- [57] K. Momma and F. Izumi, VESTA3 for three-dimensional visualization of crystal, volumetric and morphology data, *J. Appl. Crystallogr.* **44**, 1272 (2011).
- [58] R. D. Shannon, Revised effective ionic radii and systematic studies of interatomic distances in halides and chalcogenides, *Acta Crystallogr., Sect. A* **32**, 751 (1976).
- [59] S. Mugiraneza and A. M. Hallas, Tutorial: a beginner's guide to interpreting magnetic susceptibility data with the Curie-Weiss law, *Commun. Phys.* **5**, 95 (2022).
- [60] S. Singh, S. Saha, S. K. Dhar, R. Suryanarayanan, A. K. Sood, and A. Revcolevschi, Manifestation of geometric frustration on magnetic and thermodynamic properties of the pyrochlores  $\text{Sm}_2\text{X}_2\text{O}_7$  ( $\text{X} = \text{Ti}, \text{Zr}$ ), *Phys. Rev. B* **77**, 054408 (2008).
- [61] S. T. Bramwell, M. N. Field, M. J. Harris, and I. P. Parkin, Bulk magnetization of the heavy rare earth titanate pyrochlores - a series of model frustrated magnets, *J. Phys.: Condens. Matter* **12**, 483 (2000).